Compressive Imaging with Spatial Coding Masks on Low Number of Elements An Emulation Study

Hu, Yuyang ; Brown, Michael ; Doğan, Didem; Leus, Geert; Kruizinga, Pieter; Van Der Steen, Antonius F.W.; Bosch, Johannes G.

DOI
10.1109/IUS54386.2022.9957699

Publication date
2022

Document Version
Final published version

Published in
Proceedings of the IUS 2022 - IEEE International Ultrasonics Symposium

Compressive Imaging with Spatial Coding Masks on Low Number of Elements: An Emulation Study

Yuyang Hu
Biomedical Engineering, Thorax Center, Erasmus MC
Rotterdam, the Netherlands
y.hu@erasmusmc.nl

Michael Brown
Neuroscience, Erasmus MC
Rotterdam, the Netherlands
michael.brown.13@ucl.ac.uk

Didem Dogan
Micro Electronics, TU Delft
Delft, the Netherlands
D.DoganBaskaya-1@tudelft.nl

Geert Leus
Micro Electronics, TU Delft
Delft, the Netherlands
g.j.t.leus@tudelft.nl

Pieter Kruizinga
Neuroscience, Erasmus MC
Rotterdam, the Netherlands
p.kruizinga@erasmusmc.nl

Antonius F.W. van der Steen
Biomedical Engineering, Thorax Center, Erasmus MC
Rotterdam, the Netherlands
a.vandersteen@erasmusmc.nl

Johannes G. Bosch
Biomedical Engineering, Thorax Center, Erasmus MC
Rotterdam, the Netherlands
j.bosch@erasmusmc.nl

2022 IEEE International Ultrasonics Symposium (IUS) | 978-1-6654-6657-8/22/$31.00 ©2022 IEEE | DOI: 10.1109/IUS54386.2022.9957699

***Abstract*— We intend to develop an ultrasound compressive imaging device to perform carotid artery (CA) function and flow monitoring/imaging by using just a few single element transducers equipped with spatial coding masks. The spatially unique impulse responses can be exploited in compressive reconstructions. To explore the potential of different configurations, in this study we emulated such a device using a linear array system. We combined its elements with individual digital delays into a small number of groups. The results suggest our spatial coding mask approach based on reconstructions regularized with a least squares method has potential for CA monitoring with only 10 to 12 sensors.**

***Keywords*— Compressive imaging, Matched filtering, Image reconstruction, Carotid artery, Simulation**

I. Introduction

Ultrasonography of the carotid artery (CA) can non-invasively provide blood velocity, wall motion, pulse wave velocity (PWV) and vessel anatomy information which can be used as indicators of atherosclerosis[1]. Conventionally, this examination is performed by a skilled sonographer using an ultrasound system with a linear array transducer. We aim at a long-term monitoring solution for measuring functional parameters of the carotid artery such as flow and wall motion by using a patch with only a small number of ultrasound sensors.

The compressive sensing theory[2] provides possibilities for extracting information with a minimal number of sensors and observations. In a previous study[3], we proposed a compressive sensing-based method using a single channel sensor for 3D imaging. By placing an aberration mask upon the sensor we could generate a spatially coded acoustic field that allowed detailed 3D reconstructions of complex 3D objects in water.

We intend to use this compressive sensing principle to develop our carotid artery monitoring device. To explore the potential of imaging with a low number of masked sensors (Fig. 1 a), we emulated such a device using a linear array system. In this study, we only investigated the B-mode imaging potential assuming that if anatomical information is spatially reasonably separable, this should also apply to functional information such as flow and wall motion.

In the emulated system, the acoustic field inferred by the physical spatial coding (aberration) mask was translated into digital delays applied per element of the linear array (Fig. 1 c).

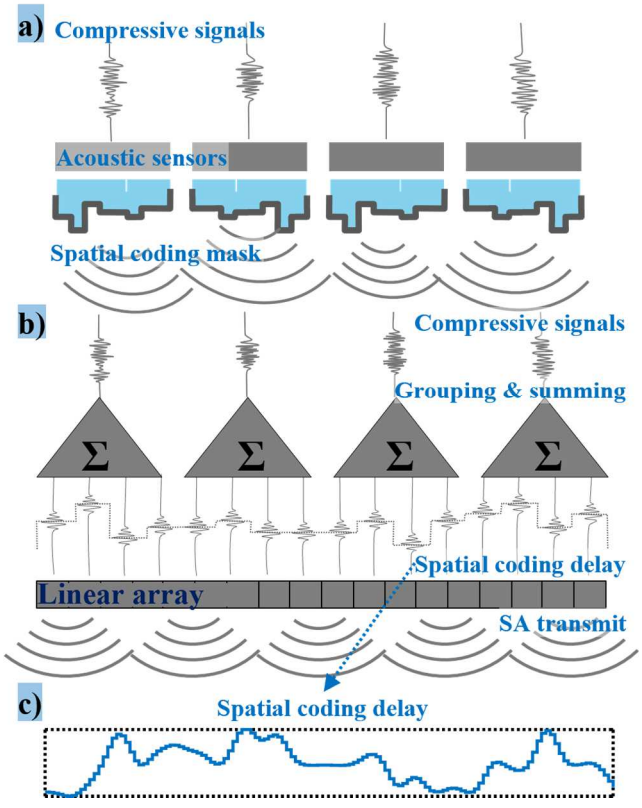

Fig. 1 a) Intended practical device. Signals are acquired by a low number of sensors with masks. b) Emulation system. Received signals from a linear array are delayed per element according to the mask pattern and summed per group. c) Fixed delay pattern was used in this study

Elements were grouped to represent a small number of sensors (Fig. 1 b). In this paper, the feasibility of our compressive sensing method in B-mode reconstruction was demonstrated, two reconstruction schemes for the compressed signals were compared, and the effect of the number of groups on the quality of the reconstruction was studied. The results will supply a lower limit for the number of sensors in a practical device design that would be sufficient to spatially separate functional information.

II. Methods

A. Emulation setup

The proposed emulation setup consisted of a 128 elements linear array transducer (L7-4) and a Vantage 256 system (Verasonics). A fixed delay mask pattern over the full aperture (randomly generated once, Fig. 1.c) was chosen to emulate the local delaying effect of the spatial coding mask in transmit and receive. The aperture was divided into equally sized groups of elements, each representing a single sensor with a coding mask. Different numbers of sensors (group sizes) were explored in this study. A synthetic aperture (SA) transmit scheme was employed when acquiring signals: each element was excited individually (4 cycles, 5 MHz) and received signals from all elements were recorded. The signal of each masked group was constructed by applying each transmit and receive element's individual delays and summing received element signals per group. The emulation system was deployed in a tissue mimicking phantom (CIRS 040GSE) and raw signals from a depth range of 5-50 mm were acquired, corresponding to a typical region of interest for carotid artery imaging.

B. Signal model

In our compressive reconstructions, a basic linear system model is employed to describe the generation of the received signals:

$$\begin{pmatrix} \boldsymbol{y}_{(1,1)} \\ \vdots \\ \boldsymbol{y}_{(t,r)} \\ \vdots \\ \boldsymbol{y}_{(N,N)} \end{pmatrix} = \begin{pmatrix} \boldsymbol{A}_{(1,1)}(1,1) & \cdots & \boldsymbol{A}_{(1,1)}(n_x,n_z) \\ & \ddots & \\ \vdots & \boldsymbol{A}_{(t,r)}(x,z) & \vdots \\ & \ddots & \\ \boldsymbol{A}_{(N,N)}(1,1) & \cdots & \boldsymbol{A}_{(N,N)}(n_x,n_z) \end{pmatrix} \begin{pmatrix} \boldsymbol{x}(1,1) \\ \vdots \\ \boldsymbol{x}(x,z) \\ \vdots \\ \boldsymbol{x}(n_x,n_z) \end{pmatrix}$$

This model relates the received element signals $\boldsymbol{y}$ to the presence of scatterers in any spatial location (expressed in $\boldsymbol{x}$) via a matrix $\boldsymbol{A}$. The matrix $\boldsymbol{A}$ contains for each index (x,z) the expected sensor signals associated with a scatterer present in that spatial position (x,z), where n_x and n_z are the number of positions/pixels in the x and z dimension of the region of interest (ROI). If the spatial signals are sufficiently unique and/or the number of observed signals is large enough, the spatial scatterer distribution can be reconstructed with reasonable spatial separation. In the case of a synthetic aperture transmit scheme on all individual elements of the linear array, $\boldsymbol{y}$ will contain in total $N \times N$ signals, where N=128 is the number of elements. Each index (t,r) in the $\boldsymbol{y}$ vector corresponds to the received signal on element r as a result of a transmit on element t. Each $\boldsymbol{y}_{(t,r)}$ also has its corresponding $\boldsymbol{A}_{(t,r)}$ in the $\boldsymbol{A}$ matrix.

When we group individual elements into a lower number of sensors for our emulation, the linear system model is very similar, but now $\boldsymbol{y}$ and $\boldsymbol{A}$ are constructed per sensor. We assume synthetic aperture transmission per sensor st and receive on each sensor sr:

$$\begin{pmatrix} \boldsymbol{y}_{(1,1)} \\ \vdots \\ \boldsymbol{y}_{(st,sr)} \\ \vdots \\ \boldsymbol{y}_{(M,M)} \end{pmatrix} = \begin{pmatrix} \boldsymbol{A}_{(1,1)}(1,1) & \cdots & \boldsymbol{A}_{(1,1)}(n_x,n_z) \\ & \ddots & \\ \vdots & \boldsymbol{A}_{(st,sr)}(x,z) & \vdots \\ & \ddots & \\ \boldsymbol{A}_{(M,M)}(1,1) & \cdots & \boldsymbol{A}_{(M,M)}(n_x,n_z) \end{pmatrix} \begin{pmatrix} \boldsymbol{x}(1,1) \\ \vdots \\ \boldsymbol{x}(x,z) \\ \vdots \\ \boldsymbol{x}(n_x,n_z) \end{pmatrix}$$

where M is the number of sensors after grouping (M<<N). The coding effect of the spatial coding mask is converted to a temporal delay per element for each $\boldsymbol{y}_{(t,r)}$ and $\boldsymbol{A}_{(t,r)}$. The corresponding sensor signals $\boldsymbol{y}_{(st,sr)}$ and sub-matrix entries $\boldsymbol{A}_{(st,sr)}$ for each group are represented by one summed temporal signal, respectively.

C. Reconstruction methods

A regular matrix inversion is not applicable to solve $\boldsymbol{x}$ (our desired image content), since the problem is highly underdetermined ($M^2 \ll n_x n_z$). Therefore, we revert to reconstruction methods that will provide an approximation of $\boldsymbol{x}$. We will employ a matched-filtering reconstruction as basic method, and we will investigate whether least-squares iterative regularization can improve the reconstruction.

a) Matched filtering method (MF):

A matched filtering method was performed as our basic reconstruction method:

$$\hat{\boldsymbol{x}}_{MF} = \sum_{st}^{M} \sum_{sr}^{M} \left(\boldsymbol{A}_{(st,sr)}^{H} \boldsymbol{y}_{(st,sr)} \right)$$

TABLE I FWHM OF PSF (MEAN (±SD)) AND CR FOR DIFFERENT RECONSTRUCTION SCHEMES AND NUMBERS OF SENSORS

Reconstruction schemes		no mask		with mask			
	Number of sensors	128 (GT)	16	16	12	10	8
MF	Lateral FWHM [mm]	0.39(±0.1)	1.68(±0.34)	0.52(±0.07)			
	Axial FWHM [mm]	0.75(±0.04)	1.08(±0.05)	1.05(±0.06)			
	CR [dB]	16.64	12.85	11.73			
LSQR	Lateral FWHM [mm]		0.78(±0.17)	0.43(±0.06)	0.53(±0.13)	0.55(±0.15)	0.49(±0.08)
	Axial FWHM [mm]		0.91(±0.05)	0.89(±0.07)	0.99(±0.12)	1.13(±0.24)	1.21(±0.31)
	CR [dB]		13.09	9.94	9.22	8.24	5.67

This publication is part of the project TOUCAN (with project number 17208) of the OTP research programme which is financed by the Dutch Research Council (NWO).

In this method, the Hermitian matrix is used as a best replacement of the intractable matrix inversion [4]. The MF method was deployed on signals from each pair of transmit and receive sensors individually (synthetic aperture per sensor) to gain better reconstruction quality with the highest possible number of observations and then summed to provide $\hat{\boldsymbol{x}}_{MF}$ as the estimation of the real $\boldsymbol{x}$ vector.

b) Least-squares method (LSQR):

The least-squares method (LSQR algorithm) [5] was investigated and compared with $\hat{\boldsymbol{x}}_{MF}$:

$$min \left\| \sum_{st}^{M} \sum_{sr}^{M} \left(\boldsymbol{A}_{(st,sr)} \hat{\boldsymbol{x}}_{LSQR} - \boldsymbol{y}_{(st,sr)} \right) \right\|_2$$

An iterative general error minimization between $\boldsymbol{A}_{(st,sr)}\hat{\boldsymbol{x}}_{LSQR}$ and $\boldsymbol{y}_{(st,sr)}$ among all observations was performed, which would lead to a $\hat{\boldsymbol{x}}_{LSQR}$ closer to the actual $\boldsymbol{x}$. In this work, the regularization was stopped after 20 iterations. In our experience, the gain of image quality was becoming insignificant at that stage.

D. Evaluation

In this study, we investigated the effects of different numbers of sensors and the reconstruction methods on B-mode image quality in our emulation setup. This should give an indication what minimal number of sensors would still properly separate information spatially, to be used in a practical monitoring device for carotid function. We investigated spatial separability in terms of lateral and axial point spread functions of wire targets, and contrast ratio of inclusions to the background

Performance of the reconstruction schemes was first compared for the case of a relatively high number of sensors

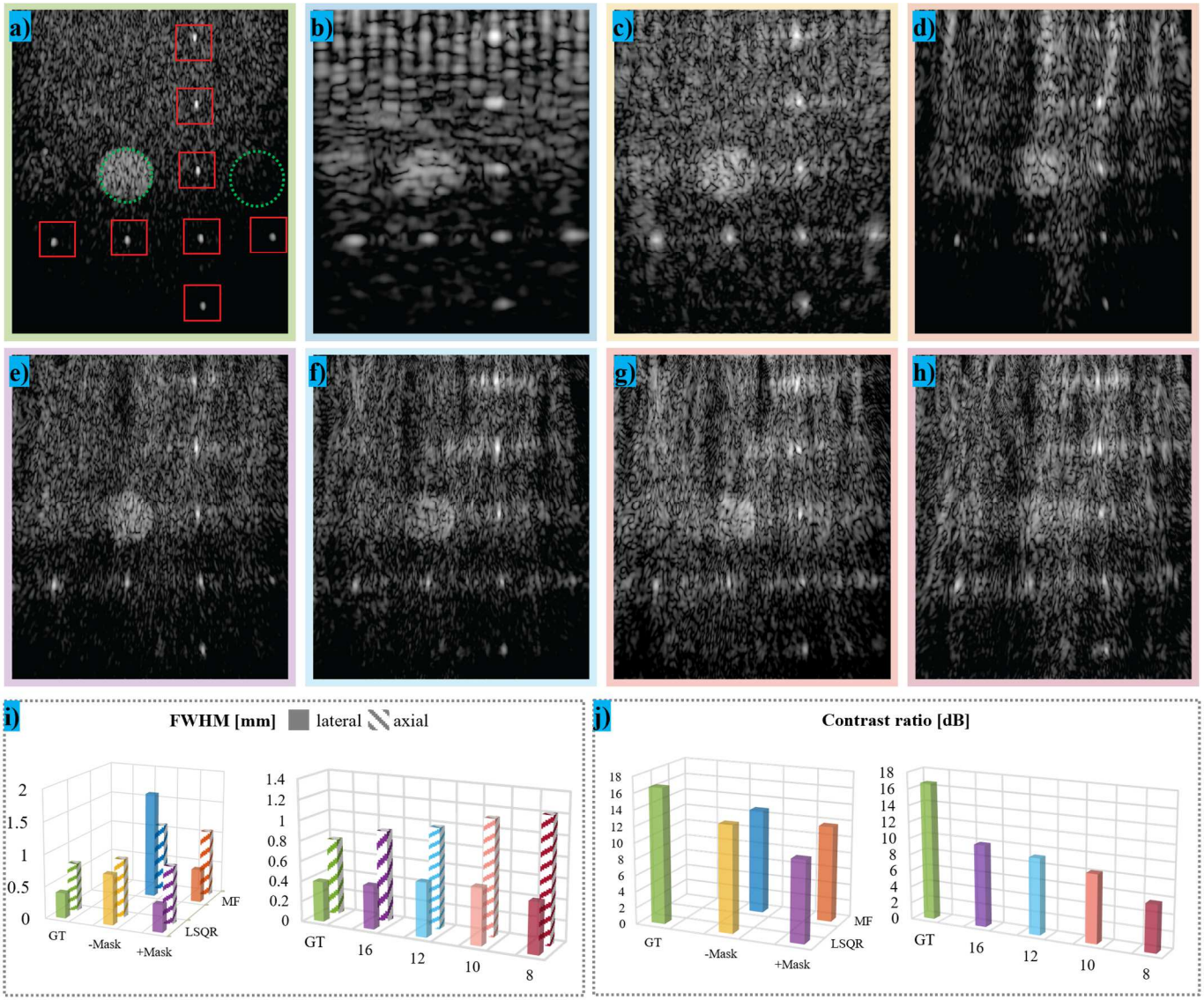

Fig. 2 Comparison of reconstructions for different methods and numbers of sensors. a) MF reconstruction with 128 sensors' signals with no mask (ground truth). FWHM of PSF was determined for the red boxes, CR from the green circles; b-e) reconstruction from 16 sensors by different schemes: b) MF with no mask; c) LSQR with no mask; d) MF with mask; e) LSQR with no mask; f-g) LSQR reconstruction using mask, with different numbers of sensors: f) 12 sensors; g) 10 sensors; h) 8 sensors; i) FWHM of lateral and axial PSF of a-e (left) and a, e-h (right); j) CR of a-e (left) and a, e-h (right).

(16), to ensure the reconstruction differences would be more distinct. The 128 elements of the total aperture were evenly divided into 16 sensors (with 8 grouped elements in each sensor). Two reconstruction schemes: with/without mask and with MF/LSQR were deployed in all four combinations on these grouped sensor's signals to determine if the use of the mask and/or LSQR improved the reconstruction. The ground truth in this study was the MF reconstruction from all 128 element signals without mask and LSQR, which was equivalent to the reconstruction by the standard synthetic aperture delay and sum method. The reconstruction quality of different schemes was evaluated by:

- Quantifying the average lateral and axial full width at half maximum (FWHM) of point spread function (PSF) of 8 wire targets in the ROI (red boxes in Fig. 2 a).
- Quantifying the contrast ratio (CR) of the inclusion region in the ROI to the background region (green dashed circles in Fig. 2 a).

The reconstruction performance for different numbers of sensors was also studied. Since the number of independent observations in Y is related to the square of the number of sensors in our synthetic aperture scheme, reducing the number of sensors should significantly affect the reconstruction quality. However, to keep our device design simple we strive for a minimal number of sensors that still allows sufficient spatial separability.

The 128 elements were evenly divided into 16, 12, 10 and 8 sensors, while in the 12 and 10 sensors case, 8 elements on the right edge of the aperture were abandoned to ensure an even division. One should realize that changing the number of sensors will also change the size of each sensor. Therefore, the effects of the number of observations and size/pitch of the sensors were studied together in this work. The reconstruction scheme that performed best in the previous part of the study (LSQR with mask) was adopted here. Reconstruction quality was evaluated in the same way as in the previous part (PSF and CR vs. GT).

III. Result

A. Reconstruction schemes

We can see in Table I and Fig. 2 a, that the ground truth reconstruction with 128 sensors had the best quality, as expected. When the number of sensors is decreased to 16, using MF without mask (Fig. 2 b), the wire targets and inclusion are still distinguishable, but the image resolution was heavily degraded and a stripy pattern appeared in the near field. The wire target PSFs were clearly improved after applying the mask and LSQR separately (Fig. 2 c, d) and even more when combining mask and LSQR (Fig. 2 e). The resulting image was visually already close to the ground truth image. Specifically, the lateral PSF was improved most by the combination of mask and LSQR. The axial PSF was slightly improved, mainly by applying LSQR. The CR slightly decreased by applying mask and applying mask with LSQR.

B. Different numbers of sensors

As we can see in Fig. 2 e-h and Table I, the reconstruction quality decreases considerably for a lower number of sensors, likely due to the lower number of observations. The axial PSF was degraded somewhat. For the lateral PSF, the degradation was minor. The CR decreased considerably, which can also be observed visually at the inclusion region. The reconstruction of the inclusion region was more sensitive to the change of the number of sensors than the reconstruction of the wire targets. But since this region is already reasonably distinguishable with 12 to 10 sensors (Fig. 2 f, g), we consider these numbers of sensors in principle useful for our purpose.

IV. Conclusion

In this emulation study, it was found that MF reconstruction from signals of a low number of masked sensors does benefit (in terms of axial and lateral PSF) from the use of a spatial coding mask. Moreover, the quality of the reconstruction can be further improved by LSQR regularization, which also fixed the uneven distribution of image intensity in the MF with mask reconstruction. However, a minor decrease in CR was seen with respect to the ground truth, which might also be related to the lower image resolution. The reconstruction with different numbers of sensors showed that a smaller number of sensors degraded the reconstruction quality mainly in axial PSF and CR. More importantly, this study also implies that for a practical device with the proposed aperture (38 mm), 12 to 10 sensors could be adequate for a reasonable B-mode reconstruction.

In this paper, only one randomly generated coding pattern was adopted, which might still be optimized towards our application scenario. Our previous work[6] has shown that this may improve results further. Furthermore, we are aiming to apply our device for flow/function monitoring in the carotid artery, for which the requirements of spatial separability might be more lenient than for B-mode imaging. These questions will be studied in our future work.

References

[1] P. M. Nabeel, V. R. Kiran, J. Joseph, V. V. Abhidev, and M. Sivaprakasam, "Local Pulse Wave Velocity: Theory, Methods, Advancements, and Clinical Applications," *IEEE Rev Biomed Eng*, vol. 13, pp. 74–112, 2020, doi: 10.1109/RBME.2019.2931587.

[2] C. E. Shannon, "A Mathematical Theory of Communication," *Bell System Technical Journal*, vol. 27, no. 3, pp. 379–423, Jul. 1948, doi: 10.1002/j.1538-7305.1948.tb01338.x.

[3] P. Kruizinga *et al.*, "Compressive 3D ultrasound imaging using a single sensor," *Sci Adv*, vol. 3, no. 12, 2017, doi: 10.1126/sciadv.1701423.

[4] G. Turin, "An introduction to matched filters," *IEEE Trans Inf Theory*, vol. 6, no. 3, pp. 311–329, Jun. 1960, doi: 10.1109/TIT.1960.1057571.

[5] C. C. Paige and M. A. Saunders, "LSQR: An Algorithm for Sparse Linear Equations and Sparse Least Squares," *ACM Transactions on Mathematical Software*, vol. 8, no. 1, pp. 43–71, Mar. 1982, doi: 10.1145/355984.355989.

[6] P. van der Meulen, P. Kruizinga, J. G. Bosch, and G. Leus, "Coding Mask Design for Single Sensor Ultrasound Imaging," *IEEE Trans Comput Imaging*, vol. 6, pp. 358–373, 2020, doi: 10.1109/TCI.2019.2948729.